A closed-loop recycling process for discontinuous carbon fibre polyamide 6 composites

*Rhys J. Tapper[1], Marco L. Longana[*1], Ian Hamerton[1], Kevin D. Potter[1]*

1 Bristol Composites Institute (ACCIS), School of Civil, Aerospace, and Mechanical Engineering, Queen's Building, University of Bristol, University Walk, Bristol, BS8 1TR, United Kingdom

[*] To whom correspondence should be addressed: m.l.longana@bristol.ac.uk.

www.bristol.ac.uk/composites

Abstract

The effects of a closed-loop recycling methodology are evaluated for degradation using a discontinuous carbon fibre polyamide 6 (CFPA6) composite material. The process comprises two fundamental steps: reclamation and remanufacture. The material properties are analysed over two recycling loops, and CFPA6 specimens show a total decrease of 39.7 % (± 3.5) in tensile stiffness and 40.4 % (± 6.1) in tensile strength. The results of polymer characterisation and fibre analysis suggested that the stiffness reduction was likely due to fibre misalignments primarily caused by fibre agglomerations, as a result of incomplete fibre separation, and by fibre breakages from high compaction pressures. The ultimate tensile strain was statistically invariable as a function of recycling loop which indicated minimal variation in polymer structure as a function of recycling loop. To the authors' best knowledge, the mechanical performance of the virgin CFPA6 is the highest observed for any aligned discontinuous carbon fibre thermoplastic composites in the literature. This is also true for recycled specimens, which are the highest observed for any recycled thermoplastic composite, and, for any recycled discontinuous carbon fibre composite with either thermosetting or thermoplastic matrices.

Keywords: Recycling; Polymer-matrix composites (PMCs); Compression moulding; Discontinuous reinforcement.

1. Introduction

Landfill is the standard waste management method for carbon fibre reinforced polymers (CFRP), however it is becoming increasingly unfavourable due to environmental, societal, and economic pressure [1]. Growing social awareness of climate change, and an industrial recognition of the impending composite waste problem, led to the development of environmental legislature that

regulates the recyclability of modern structures [2]. The development of recycled CFRP (rCFRP), and processes with which to recycle them, has attracted increased research interest in the last decade [3]. Over this period there have been three comprehensive reviews of the available technologies and future outlook: Pickering in 2006 [4], Pimenta & Pinho in 2011 [5] and Oliveux *et al.* in 2015 [6].

It is apparent that there is a need to develop a sustainable production cycle for CFRP that fits into the Circular Economy paradigm, developed by the Ellen MacArthur Foundation [7] and supported by the UK Composite strategy for future composite material production [8]. It is therefore equally important to recycle with the intent of finding a valuable application for the recyclate fibre and matrix. The development of a recycling process able to produce a high-value, structural rCFRP goes a long way towards closing the loop for CFRP manufacture, and meeting the requirements of a circular economy paradigm. The term recycling here describes the reclamation of constituents from waste composites and the subsequent remanufacture into useful composite components of value.

The current thermoset material paradigm is not conducive to closed-loop recycling due to the currently unavoidable degradation of the thermoset matrix required to reclaim fibres, leaving potentially up to 50 % of the composite volume un-recycled. Thermoplastic matrices present a unique opportunity for recycling, as the molecular structure can be temporarily dissociated using heat or solvent treatment, *i.e.* through dissolution. Melt recycling causes a significant reduction in mechanical properties due to fibre breakage and matrix degradation during processing as a result of the high temperatures and shear forces required for extrusion and injection moulding [9]. The dissolution/precipitation technique involves the dissolution of a thermoplastic in a solvent at a given temperature. Once in solution, the polymer can potentially be separated from reinforcement by filtration and subsequently reclaimed by precipitation following the addition of a destabilising non-solvent [10,11]. This method has been applied to polystyrene [12], low density polyethylene and high density polyethylene [13,14], with the aim of providing a selective sorting process for mixed municipal wastes, and for recycling un-reinforced PA6, and PA66 [10]. It had not been applied to fibre reinforced polymers until a recent study where it was adapted for CF polypropylene (CFPP) composites [15]. The study showed that CFPP composite could be recycled using an equivalent closed-loop recycling process without any reduction in mechanical properties. The mechanical performance achieved was superior to alternative discontinuous CFPP composites, however it was lower than the requirement for high-value applications such as semi-structural automotive parts.

This study aims to improve the previous closed-loop recyclable material, and associated recycling process, by incorporating a matrix of increased mechanical performance, *i.e.* polyamide 6 (PA6). This will provide a recyclable composite of enhanced mechanical performance that is applicable to a wider range of high-value applications. Without a high-performance, high-value

application for rCFRP the closed-loop production paradigm, and thus the stable recycling infrastructure, cannot be realised. PA6 was used as the thermoplastic in this study due to the following advantages: It is a semi-crystalline thermoplastic that is soluble in low-hazard solvents; It can provide higher composite mechanical performance than polypropylene, due to increased matrix tensile stiffness, strength, and interfacial shear strength with CF; It has the best compromise of mechanical properties and processing temperature out of the other polyamide variants, *i.e.* higher mechanical performance than polyamide 12 and lower processing temperatures than polyamide 66; PA6 is commercially available and comparative composite data is available as CFPA6 have been widely evaluated in the literature [9,16,25–31,17–24]; The industrial applicability is demonstrated by its commercial availability [32].

2. Materials and Methods

2.1 Materials

Virgin PA6 (vPA6) was sourced in powder form from Goodfellow distributors. The material properties of vPA6, as determined through in-house polymer characterisation, can be found in Table 1. PA6 was selected as the matrix for the reasons specified above.

Table 1. Properties of the polyamide 6 used in this study.

	Density	T_m	T_g	X	M_W	M_n	PDI
	g/cm3	°C	°C	%	g/mol.	g/mol.	-
PA6	1.13	217	45.0	34.9	5.53 x 104	7.83 x 103	7.70

X = crystallinity

Discontinuous CFs used in this study were supplied by TohoTenax (standard type C124). The TohoTenax fibres were 3 mm in length and came with a proprietary water-soluble sizing (3.8 wt.%) used to aid dispersion in the alignment carrier liquid. 3 mm CF were used as they are the optimum length for alignment using the HiPerDiF, are less prone to breakages than long fibres, and are similar in form to rCFs. Material properties of the CFs used can be found in Table 2. Reagent grade benzyl alcohol and acetone were sourced from Alfa Aesar and Fisher Scientific, respectively.

Table 2. Properties of the carbon fibres used in this study.

	Length	Density	Diameter	E_T	σ_T	e
	mm	g/cm^3	µm	GPa	MPa	%
CF	3	1.82	7	225	4344	1.93

Material properties sourced from literature [33]

2.2 *Experimental methods*

2.2.1 *Introduction*

The closed-loop recycling methodology is represented schematically in

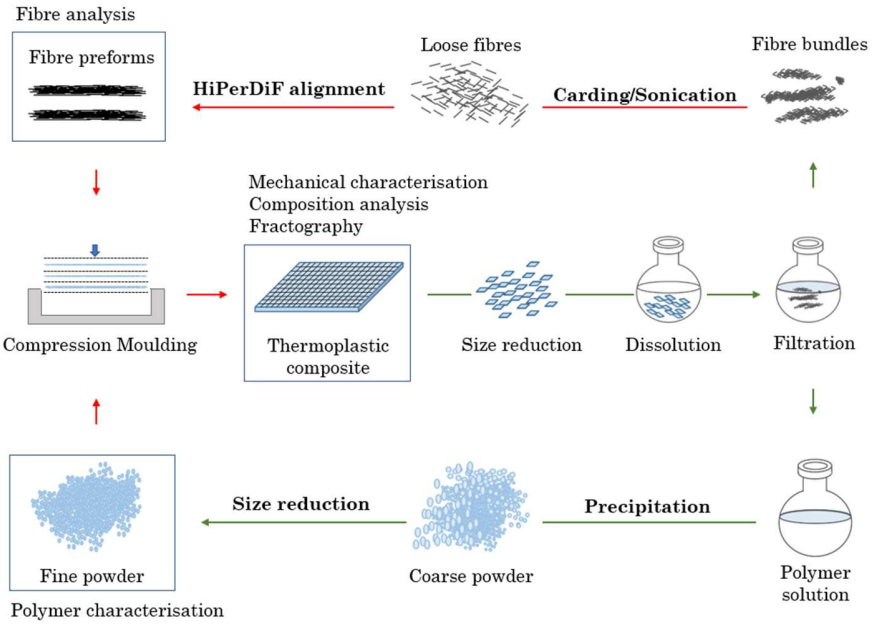

Figure 1, complete with annotations indicating the stage where material characterisation occurred. The virgin CFPA6 specimens (vCFPA6) were manufactured from virgin constituents and mechanically tested. vCFPA6 specimens were then washed, chopped and reclaimed using benzyl alcohol as solvent and acetone as non-solvent, compliant with the dissolution/precipitation technique. Fibres were filtered from the matrix solution, after this each constituent followed separate reclamation and remanufacturing paths, these are detailed in later sections. Constituents were remanufactured into specimens analogous to the virgin composite, requiring no additional fibre or matrix, and the cycle was continued for a total of two loops resulting in two recycled specimens, r_1CFPA6-BA and r_2CFPA6-BA. The method was developed to minimise property degradation, as the aim was to reclaim high-quality constituents then remanufacture these into high performance components after multiple cycles.

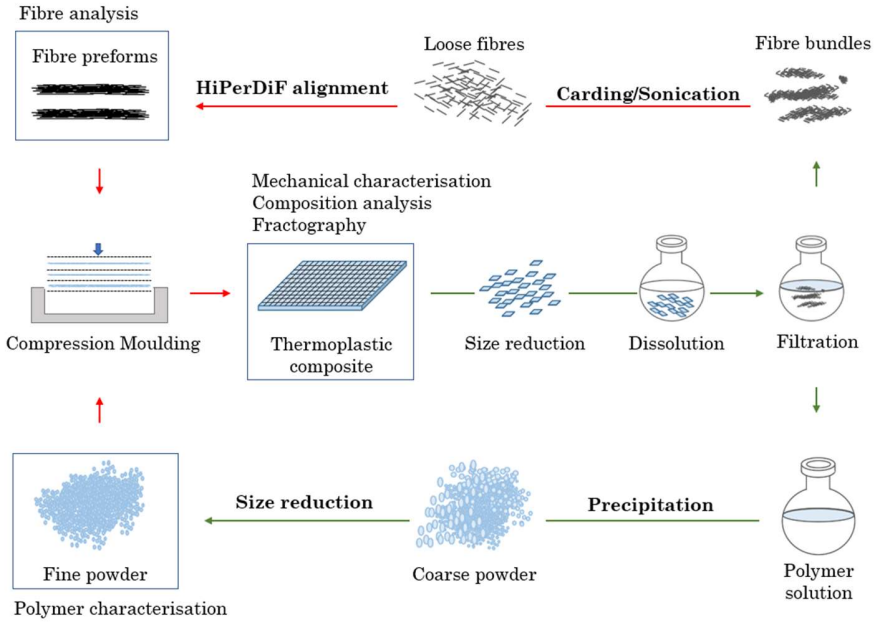

Figure 1. The closed-loop recycling method used with material characterisation annotation. The green and red arrows represent the reclamation and remanufacturing procedures, respectively.

2.2.2 Composite reclamation

Experimental parameters used in the reclamation process, can be found in Table 3. Full dissolution of PA6 occurred in benzyl alcohol at 160 °C after 1 hour. Volumes of solvent and non-solvent are dependent on the mass of PA6 in the waste feedstock. The key stage of reclamation was the separation of fibres from the polymer solution. rCFs were filtered at 25 °C and rCFs were dried in a vacuum oven (~ - 29 inHg) at 80 °C for 14 hours.

Table 3. Reclamation parameters used for carbon fibre polyamide 6 (CFPA6) recycling.

	Solvent	Temp.	Time	Non-solvent	Conc.	Solvent Ratio	Fibre Yield
	-	°C	mins	-	% w/v	S:NS	%
CFPA6-BA	benzyl alcohol	160	60	acetone	1	1:1	96

Temp. = Temperature, Conc. = Concentration, S:NS = solvent : non-solvent

The benzyl alcohol solvent system required dissolution at elevated temperatures, which increased the energy demand of recycling. However, elevated temperatures may result in a comparatively faster dissolution rate to other systems. The disparity in boiling point between solvent and non-solvent enables reclamation through fractional distillation. An alternative solvent system was tested, using formic as solvent with water as the non-solvent. This system can provide full dissolution at room temperature, which reduces the recycling process energy demand; this may become substantial at scaled volumes. However, this afforded a

decreased dissolution rate and caused solvent reclamation issues through incomplete separation, as the boiling points of the two solvents are very similar and formed an azeotropic mixture. The latter cannot be separated directly by boiling point, but can be separated by more complex separation methods, such as continuous reactive distillation or salt distillation, where the boiling point/vapour pressure of one component is varied to enable distillation [34]. These require additional materials and additional processes to provide solvent reclamation, which will likely increase the energy demand of reclamation and ultimately costs.

The rCF bundles were separated by the following wet sonication method. CFs (*ca.* 100 mg) were suspended in a beaker containing water (1 L) placed in an ultrasonic bath. Stirring separated most fibres however some agglomerations required additional manual separation. PA6 was precipitated by cooling to room temperature and the addition of acetone at a 1:1 volume ration. The precipitate was vacuum filtered using Buchner apparatus, washed and dried in a vacuum oven (~ - 29 inHg) at 80 °C for 14 hours. vPA6 and the reclaimed precipitates, r_1PA6-BA and r_2PA6-BA, underwent polymer characterisation to determine the effects of recycling on the polymer structure.

2.2.3 Composite re-manufacture

Dried rCF were aligned into dry preforms using the HiPerDiF alignment method. Alignment produced highly aligned, dry, rCF preforms with an area of 100 mm x 5 mm. The preform areal weight varied due to intrinsic, experimental variations of the HiPerDiF alignment method, however, the average total preform mass for each specimen was approximately 105 mg. Fibre analysis was carried on the vCF and both batches of reclaimed CFs, r_1CFPA6-BA and r_2CFPA6-BA. The rCF preforms, and polymer precipitate, were combined in an alternating ABA stacking sequence so that each composite stack was made up of 4 preform layers and 3

matrix layers. The remanufacture tract of

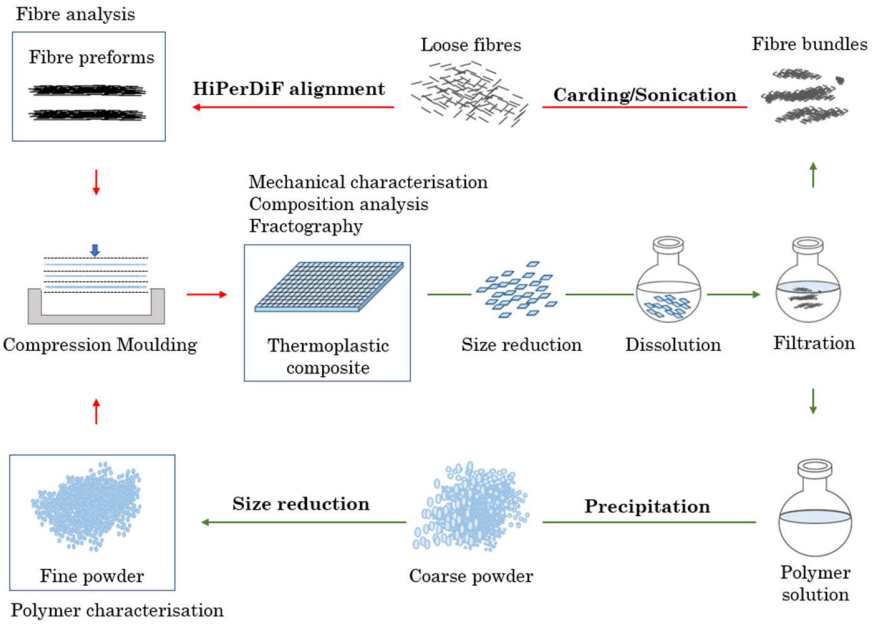

Figure 1 exhibits a representative cross-section of a composite stack in the *xy* plane. Six composite stacks were laid separately in an aluminium tool with six individual cavities of dimensions: 1 mm × 5 mm x 100 mm, this resulted in six composite specimens of equivalent dimensions to the cavity after consolidation and cooling. The compression moulding cycle, conducted in a vacuum bag to remove the catalytic effects of atmospheric oxygen, is plotted in Figure 2. Additional remanufacturing variables are reported in Table 4. Composition analysis, mechanical characterisation and fractography was carried out on virgin composite specimens and recycled composite specimens, r_1CFPA6-BA and r_2CFPA6-BA.

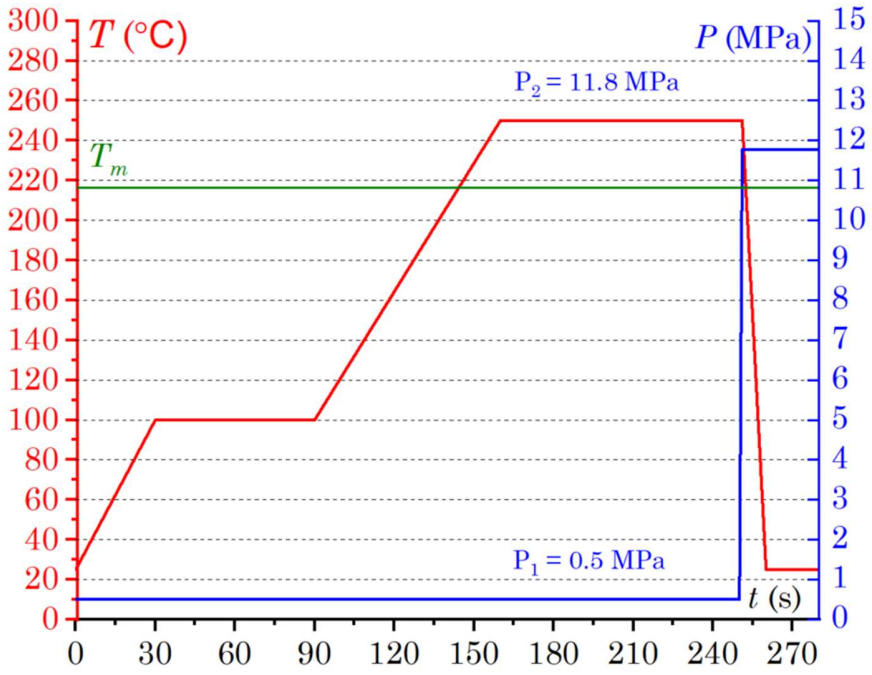

Figure 2. Compression moulding cycle used to manufacture carbon fibre polyamide 6 specimens. Specimens were held at 0.5 MPa (P1) for 4 hours until transfer from oven to hot press for consolidation at 11.8 MPa (P2). T_m denotes the melting temperature of polyamide 6.

Table 4. Remanufacturing parameters used for carbon fibre polyamide 6 (CFPA6) recycling.

	CF mass	PA6 mass	Temp.	Pressure	Actual Vf_F	Flash
	mg	mg	°C	MPa	%	wt.%
CFPA6	105[a]	180[a]	250	11.8	28	11

[a] Per specimen, Temp. = Temperature

The dominance of matrix and fibre contributions to the overall composite behaviour could be determined by combining vCF with reclaimed matrix and *vice versa*. A constituent exclusion study was carried out to test these contributions. This study used a variation of the typical closed-loop process formats, manufacturing composite specimens using: vPA6 with second iteration recycled fibres (r_2CF), and first iteration recycled PA6 (r_1PA6) with vCF. The composites produced from these conditions were denoted r_2CF.vPA6 and vCF.r_1PA6, respectively.

2.2.4 Polymer characterisation

Polymer characterisation was carried out on the vPA6 powder and the reclaimed powders after each recycling loop, *i.e.* r_1PA6-BA, and r_2PA6-BA. DSC was used to examine the effect of recycling on the melting temperature (T_m), and the percentage crystallinity (X) of the polymer, determined using equation (1) [35].

$$X = \left[(\Delta H_m - \Delta H_c) / \Delta H_m{}^0\right].100 \quad (1)$$

where ΔH_c is the enthalpy of fusion for the crystallization transition, $\Delta H_m{}^0$ is an enthalpy of fusion reference value for a pure crystal of the polymer, *i.e.* if the polymer was 100 % crystalline. The crystallization enthalpy contribution is only accounted for when a re-crystallisation event, *i.e.* annealing, occurs. For PA6, a $\Delta H_m{}^0$ of 230 J g^{-1} was used, as sourced from the literature [36]. DSC routines included two thermal ramps; the first ramp heated from 30 °C to 250 °C and cooled to 30 °C, the second ramp heated form 30 °C to 250 °C again, then cooled to room temperature. Analysis was carried out using a TA Auto Q2000 DSC in pierced, hermetically sealed aluminium pans on powdered samples (10 ± 3 mg), under flowing N_2 (50 cm^3/min), at a heating rate of 10 °C/min and cooling rate of 20 °C/min. A Perkins Elmer Spectrum 100 Fourier Transform Infrared Spectrometer was used to compare the vibrational frequencies of polymer functionalities as a function of recycling loop. The characteristic vibrations present in the fingerprint region are sufficient confirmatory evidence of the specific functional groups of PA6, and any subsequent shifts due to degradation, therefore no further spectral analysis was conducted with infra-red. M_w, M_n, polydispersity (PDI) and molecular weight distribution (MWD) of each recyclate was determined using gel permeation chromatography with size exclusion chromatography (GPC/SEC). Samples were analysed using a Malvern/Viscotek TDA 301 GPC system with associated pump and autosampler, with two PL HFIPgel 300 x 7.5 mm^2, 9 µm columns and an Agilent PL HFIPgel guard column. The mobile phase used was 1,1,1,3,3,3-hexafluoropropan-2-ol (with 25 mM NaTFAc) at 40 °C at a rate of 0.8 ml/min. A refractive index detector (with differential pressure/viscosity and right-angle light scattering) was used. Samples were prepared by adding the mobile phase (10 ml) to the sample (20 mg) to dissolve overnight. Solutions were then thoroughly mixed and filtered through a 0.45 µm PTFE membrane, directly onto autosampler vials. The vials were placed in an autosampler where injection of a vial aliquot was carried out automatically. High performance liquid chromatography with mass spectrometry (HPLC-MS) was used to qualify the extraction of any additive molecules in the reclamation supernatant, as this could be a cause of mechanical performance reduction. Specific polymer additive mixtures are typically proprietary and therefore unknown; peaks found in the spectrum were cross-referenced with known polymer additives for identification of unknown solutes. This was carried out using a Thermo Orbitrap Elite LCMA. The mass spectrometer was operated in positive ion mode at a 60k resolution with spectra being recorded between 120 and 1200 Da.

A Waters Acquity BEH C18 1.7 µm column was used for chromatography. The column was held at 5 % acetonitrile/water for 1 min (0.25 ml/min) and compounds were then eluted with a linear gradient to 95 % acetonitrile over 23 minutes before re-equilibrating the column into the starting conditions.

2.2.5 Mechanical testing

Specimens were tested for their tensile properties in accordance with ASTM D3039. Axial force was provided by a Shimadzu AGS-X servo-electric tensile test machine with a 10 kN load cell and a constant cross-head displacement of 1 mm/min. Three strain measurements were taken along the length of each specimen using an Imetrum video-gauge system, over a gauge length of 50 mm. These were averaged to produce the presented strain measurement. specimens were sprayed black and speckled with white dots to aid with strain mapping, analogous to the testing carried out in previous studies [15]. All specimens were tested with the required GFRP end tabs bonded with cyanoacrylate adhesive. Tensile specimen geometry and dimensions are reported in Table 5 and displayed in Figure 3.

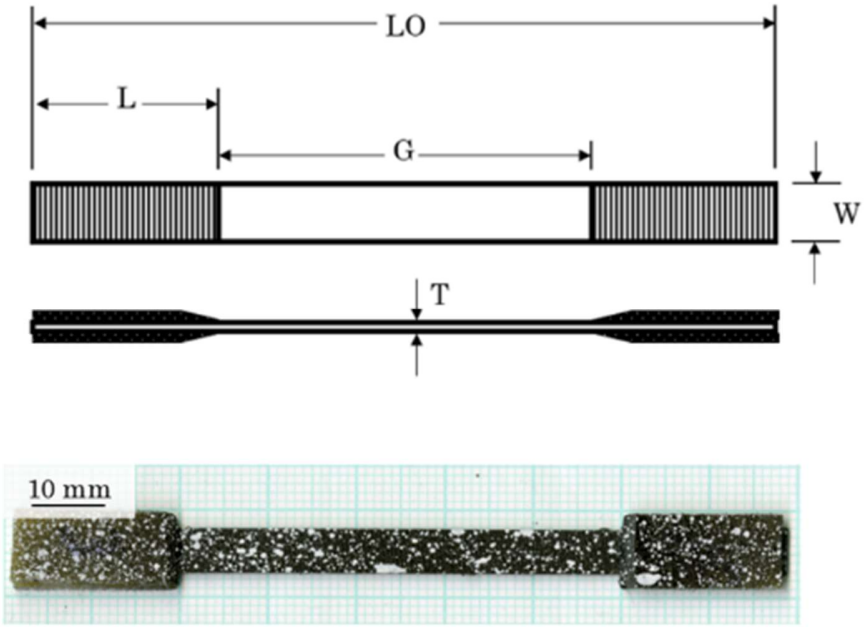

Table 5. Tensile test specimen dimensions.

	W	L	LO	G	T

	mm	mm	mm	mm	mm
CFRP	5	25	100	50	0.25-0.40

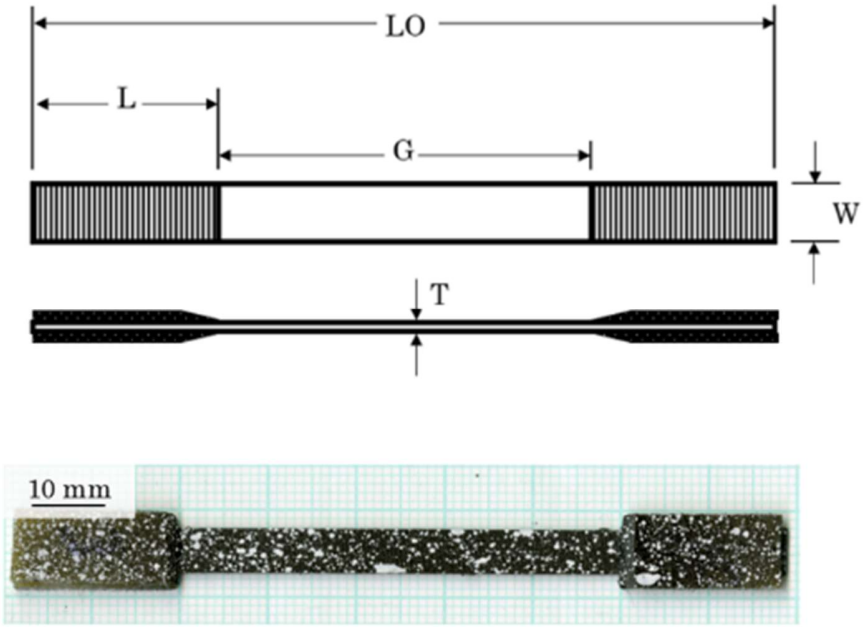

Figure 3. a) Schematic of the tensile test specimen geometry annotated with dimensions. b) composites test specimen prepped for mechanical testing.

2.2.6 Composite composition analysis

The average thickness ($\bar{t}$), and width ($\bar{w}$), of the composite specimens was measured using a micrometer; three measurements were taken at three different locations along the length and an average was taken. Volume fractions of the composite (V_C), fibres (V_{fF}), matrix (V_{fM}), and voids (V_{fV}), were calculated using the measured cross-sectional area (A_x), measured composite length (l_C), measured mass of fibre preforms (m_F), measured composite mass (m_C), calculated matrix mass (m_M), nominal fibre density (ρ_F) and matrix density (ρ_M), according to the expressions in equation (2):

$$A_x = \bar{t} \times \bar{w}, \quad V_C = l_C \times A_x, \quad m_M = m_C - m_F \tag{2}$$

$$V_{fF} = \frac{m_F}{\rho_F} \cdot \frac{100}{V_C}, \quad V_{fM} = \frac{m_M}{\rho_M} \cdot \frac{100}{V_C}, \quad V_{fV} = 1 - (\ V_{fF} + \ V_{fM})$$

Changes in V_{fF} were monitored as a function of recycling loop. It was not possible to perform any other V_{fF} measurement techniques, *e.g.* resin burn-off acid digestion or cross-sectional analysis, as they would make the materials unavailable for the subsequent recycling loops. Tensile stiffness and strength values were normalised by calculated V_{fF}.

2.2.7 Fibre analysis & fractography

Fibre surfaces were qualitatively evaluated, using a Hitachi TM3000 scanning electron microscope (SEM) with 5000 V accelerating voltage, to determine surface defects or surface deposition of matrix on fibres in the dried preform state. Fibre length distribution (FLD) analysis was carried out to determine the effects on the fibre length after each loop. A portion of each preform was cut, dispersed in water and slowly gravity filtered until an even distribution of fibres remained on filter paper. A portion of this distribution was scanned using an Epson 11000XL. Each fibre, within a consistent sample region of the high-resolution image, was measured and collated using ImageJ software. Fracture surfaces were inspected using a Hitachi TM3000 SEM (5000 V accelerating voltage). One fracture surface was examined per six specimen batch to maximise the amount of material being recycled.

3. Results and Discussion

3.1 Polymer characterisation

The DSC thermograms are overlaid in

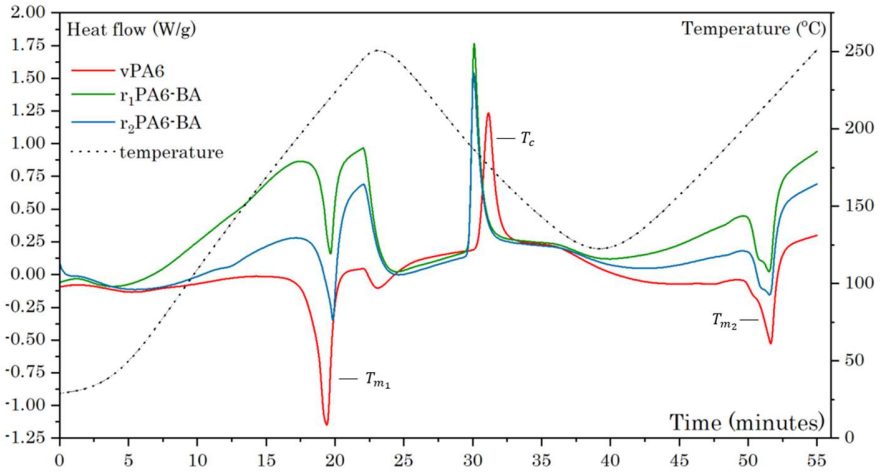

Figure 4, Melt and crystallisation temperatures are reported alongside crystallinities in Table 6. Following the x-axis from left to right, the first endothermic peak, first exothermic peak and second endothermic peak represent the initial melting (T_{m_1}), the crystallisation (T_c), and the second melting (T_{m_2}) phase transitions of the polymers. vPA6 exhibited a sharp initial melting peak at

217 °C with a crystallinity of 34.9 %. Both r_1PA6-BA and r_2PA6-BA showed a sharp T_{m_1} peak at 219 °C and 220 °C, with a crystallinity of 19.8 % and 31.1 % for the first and second recyclate, respectively.

The disparity in crystallinity can be explained by the kinetic dependency of polymer crystal formation. In solution, polymers form coils that curl back themselves in a spherical morphology called the hydrodynamic volume [37]. Upon precipitation, the coil is instantaneously forced into the solid phase giving little time for polymer chains to align and form crystal structures. Therefore, the non-linear variation in crystallinity is not surprising, and does not indicate change in the polymer chain structure. There is a second, broad melting peak after T_{m_1} in the vPA6 thermogram that is not present in the subsequent reclaimed precipitates, this suggests the extraction of a substance during the first reclamation. The crystallisation transition, at T_c, shifted from 177 °C for vPA6, to 186 °C and 187 °C for r_1PA6-BA, and r_2PA6-BA, respectively. this equates to an initial increase in the crystallinity by 23 % after the first recycling loop and a 6.3 % decrease after the second recycling loop. The second decrease in crystallinity is small and is assumed to be within the machine measurement variance, which suggests no significant change in the polymer structure. However, there is a significant change in the crystallisation behaviour after the first recycling loop. This shift can be explained as either: a) a consequence of the remanufacturing process, *i.e.* a change in the molecular weight distribution of the polymer; or b) that the polymer chains forming crystalline regions are not proximal in the un-mixed melt phase of the precipitated polymer, and thus will exhibit different crystallisation behaviour to homogenised vPA6 powder.

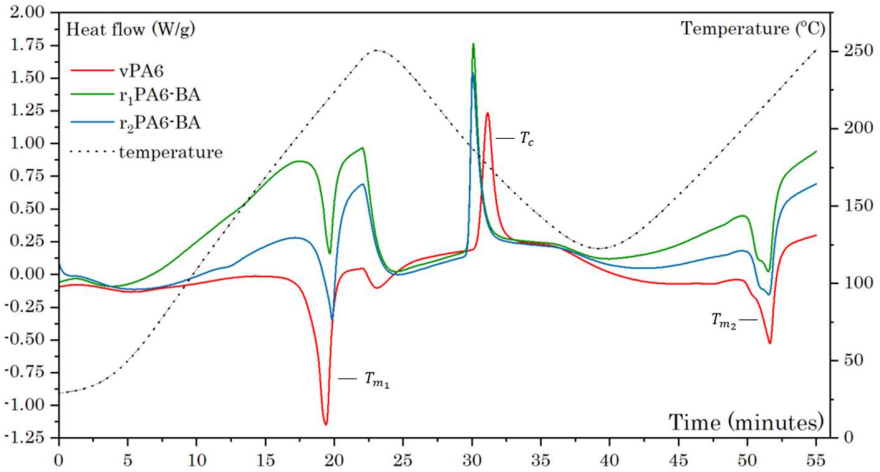

Figure 4. Multi-ramp differential scanning calorimetry thermograms for polyamide 6 as a function of recycling loop.

The final melt transition occurred at the same temperature with the same crystallinity for each sample, however, the peak splits into two broad peaks. These represent the presence of two distinct crystalline phases in the polymer that were not in vPA6. This

is a further reinforcement of the hypothesis that the instantaneous precipitation resulted in a heterogeneous spatial, *i.e.* not statistical, distribution of polymer chains, causing a significantly different crystallinities to vPA6 at the initial melting, recrystallisation and secondary melting transitions. The differences in crystallinity diminish as a function of melt transition which indicates that the differences in spatial distribution are likewise equalizing through melt processing. This also suggests that the variation in crystallinity is not a consequence of polymer degradation.

Table 6. Differential scanning calorimetry results from virgin and recycled polyamide 6 as a function of recycling loop.

	T_{m_1}	T_c	T_{m_2}	X_{m_1}	X_c	X_{m_2}
	°C	°C	°C	%	%	%
vPA6	217	177	218	34.9	24.7	20.0
r_1PA6-BA	219	186	218	19.8	30.4	20.3
r_2PA6-BA	220	187	218	31.1	28.5	18.2

The FTIR spectra collected for vPA6, r_1PA6-FA and r_2PA6-FA are overlaid in

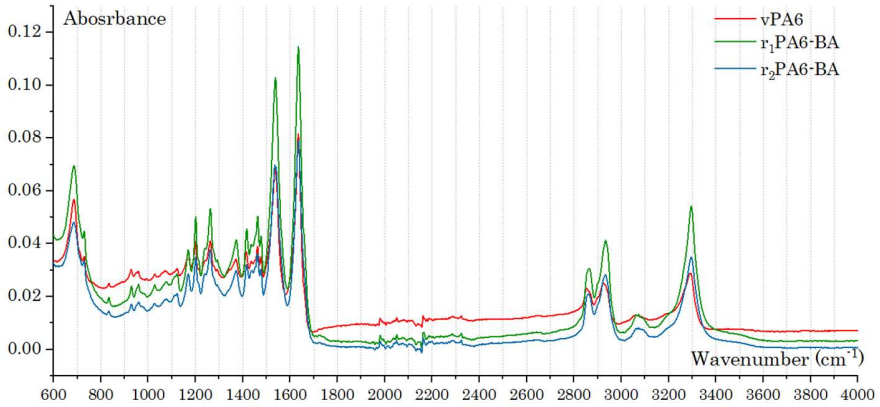

Figure 5. The characteristic vibrational peaks for PA6, using the fingerprint region profile as confirmatory evidence as sourced from the literature [31,38], were present in all specimens and are presented in Table 7. There is a weak peak at 3060 cm^{-1} which may represent a stretching vibration of crystalline hydrogen bonded -N-H [38]. As this peak refers to the crystalline, hydrogen bonded -N-H amine, it reflects the effect of reclamation on the variation in polymer crystallinity observed in the DSC thermograms. However, this is speculative and would require more detailed FTIR analytical techniques to be definitive. There are no observable peaks associated with the depolymerisation product caprolactam which suggests that either: a) any degradation that had occurred was unsubstantial; or b) that the caprolactam produced was extracted into the supernatant and did not precipitate out with the bulk polymer.

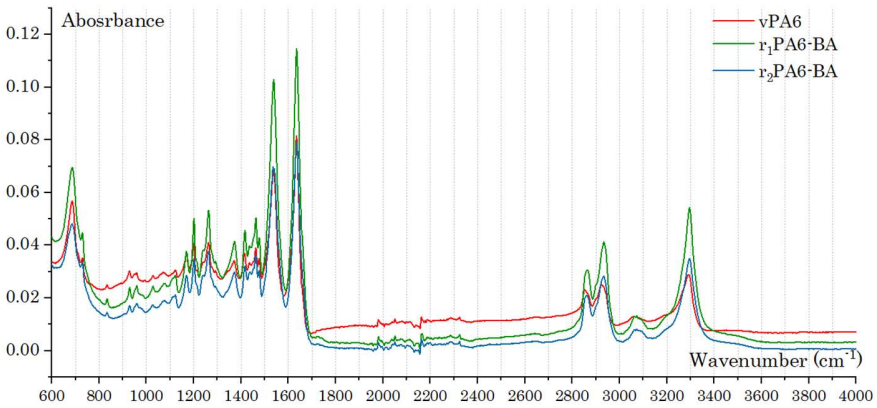

Figure 5. Fourier transform infrared spectra of polyamide 6 as a function of recycling loop.

Table 7. Vibrational peaks for polyamide 6 observed in the Fourier transform infrared spectra [31,38].

Wavenumber	Vibrational peaks
cm^{-1}	
3291	-NH symmetric stretching
2933	$-CH_2$ asymmetric stretching
2860	$-CH_2$ symmetric stretching
1637	-C=O symmetric stretching
1541	-NH symmetric bending -CN symmetric stretching
1458	$-CH_3$ symmetric bending
1419	$-CH_3$ symmetric bending
1372	-NH symmetric bending, -CN symmetric stretching, $-CH_2$ symmetric bending
684	-NH symmetric bending

The MWD curves obtained from GPC/SEC of vPA6, r_1PA6-BA and r_2PA6-BA are shown in

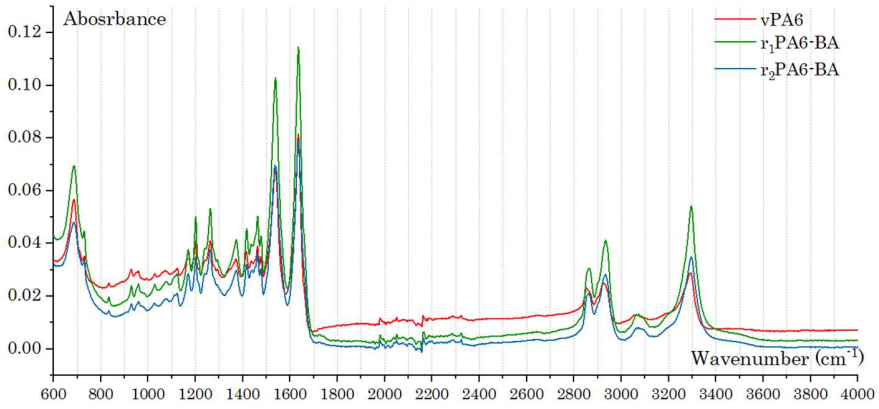

Figure 5. Fourier transform infrared spectra of polyamide 6 as a function of recycling loop., and the M_n, M_w and PDI values are tabulated in Table 8. The MWDs are representative of polydisperse semi-crystalline polymers, as expected from the PA6 used. The MWD is bi-modal, showing a primary and secondary peak. The secondary peak indicates the substantial presence of smaller molecular weight chains. This could represent the presence of an additive polymer not extracted during reclamation or, most likely, unremoved low-molecular weight, prematurely terminated PA6 by-products of step-growth polymerisation, a typical method of PA6 manufacture.

After the first recycling loop there is a 27 % and 12 % decrease in M_w and M_n, respectively. The primary peak maximum remains the same height but shifts to a lower molecular weight. This corresponds to the scission of large molecular weight chains into short lengths. The secondary peak remains unchanged, suggesting that the corresponding chains are unaffected by reclamation. After the second recycling loop, the primary peak maximum increases in height and shifts to a lower molecular weight. This represents the scission of larger chains into medium lengths and an increase in shorter chain lengths; again, the secondary peak is unaffected. Overall, the GPC analysis shows successive degradation of the primary peak but no change in the secondary peak.

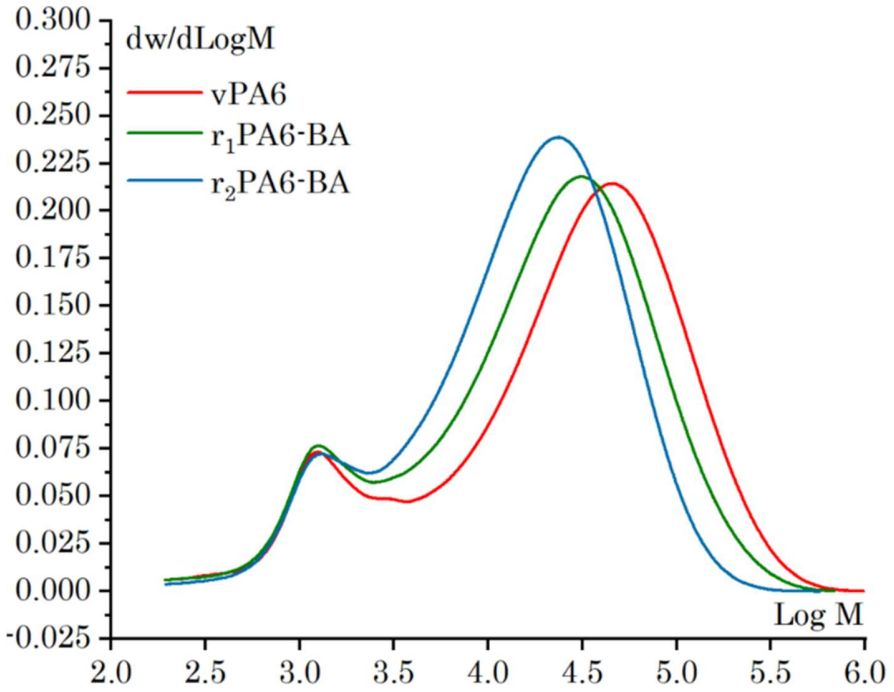

Figure 6. Molecular weight distribution from gel permeation chromatography of recycled polyamide 6 as a function of recycling loop. From left to right the plots run from low to high molecular weights.

Table 8. The M_n, M_w and poly dispersity values obtained from gel permeation chromatography of polyamide 6 as a function of recycling loop.

	M_n	M_w	PDI
	x10^3 g/mol.	x10^4 g/mol.	
vPA6	7.19 (0.1)*	5.53 (0.1)	7.69
r_1PA6-BA	6.35 (0.1)	4.01 (0.1)	6.31
r_2PA6-BA	6.38 (0.1)	2.83 (0.1)	4.43

* Coefficient of variance

The solids extracted into the supernatant after the first recycling loop were separated using HPLC and analysed using mass spectrometry (MS). The base peak chromatogram obtained is presented in

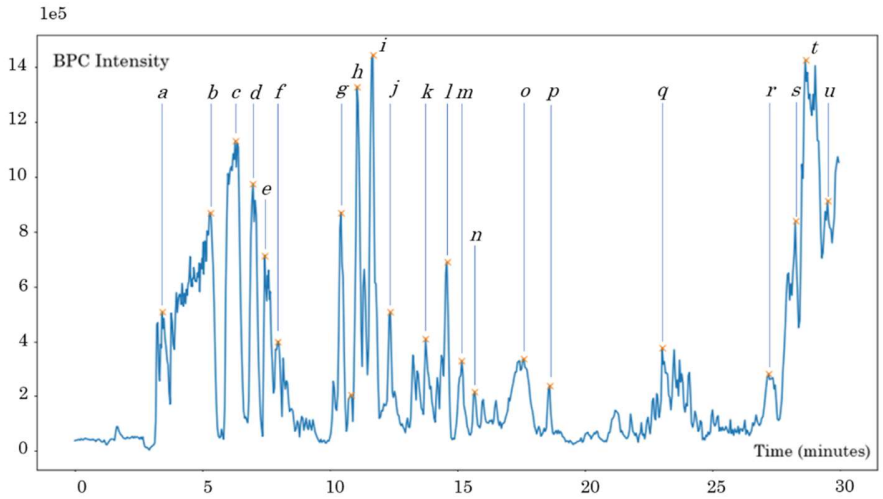

Figure 7, and the corresponding molecular mass values from MS are tabulated in

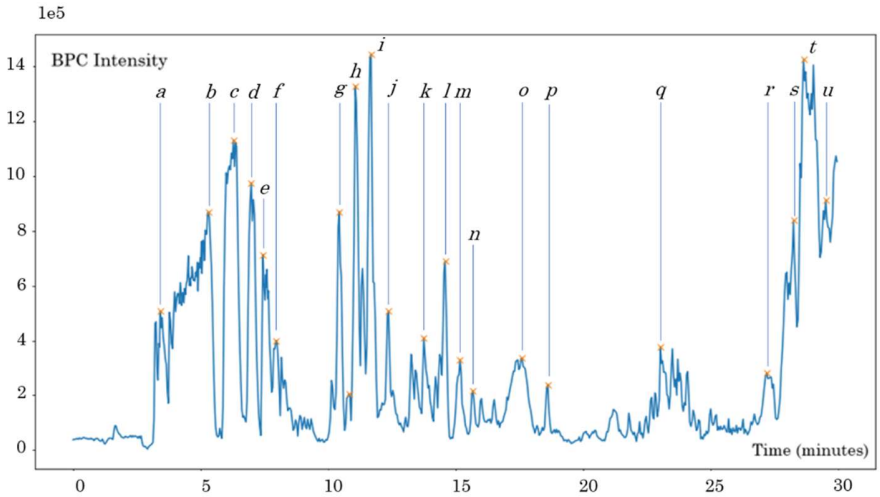

Figure 7. The base peak chromatogram (BPC) obtained from high performance liquid chromatography of the r1PA6-BA supernatant.

Table 9. The chromatogram indicates the presence of a varied mixture of compounds in a range of different quantities. These peaks represent any molecules soluble in benzyl alcohol that were not precipitated from the solution. The corresponding molecular mass values of the main chromatogram peaks are all small, < 900 g/mol, and are unlikely to be polymer chains which have larger masses by several orders of magnitude; suggesting the presence of additive molecules.

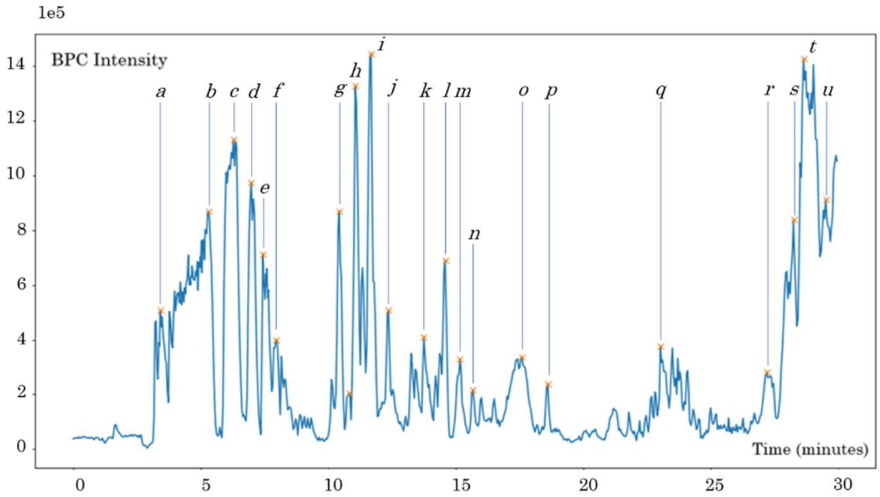

Figure 7. The base peak chromatogram (BPC) obtained from high performance liquid chromatography of the r_1PA6-BA supernatant.

Table 9. Base peak chromatogram peaks from the r_1PA6-BA supernatant with corresponding mass values from mass spectrometry.

Peak	Molecular mass	Peak	Molecular mass
	g/mol.		g/mol.
a	475.3	*k*	461.2
b	362.2	*l*	389.2
c	475.3	*m*	403.2
d	588.4	*n*	403.2
e	701.5	*o*	360.4
f	814.6	*p*	304.3
g	299.2	*q*	743.6
h	304.2	*r*	806.6
i	317.2	*s*	806.6
j	430.3	*t*	782.6
k	313.2	*u*	758.6

The additive mixtures used in polymers are generally guarded, proprietary information, however a range of known antioxidants with molecular masses ranging from 220 g/mol – 1178 g/mol. is known [39,40]. Peak *h* had a mass of 340.2 it is the mass of the known additive Antioxidant 2246 [40]. The other peaks, especially those of larger masses, must correspond to the molecular ion

peaks or fragment ions of other additives used. In any case, it is apparent that a mixture of small molecules is extracted in the reclamation supernatant.

3.1.1 Mechanical testing

Representative stress-strain curves obtained from tensile tests of CFPA6-BA as a function of recycling loop are shown in

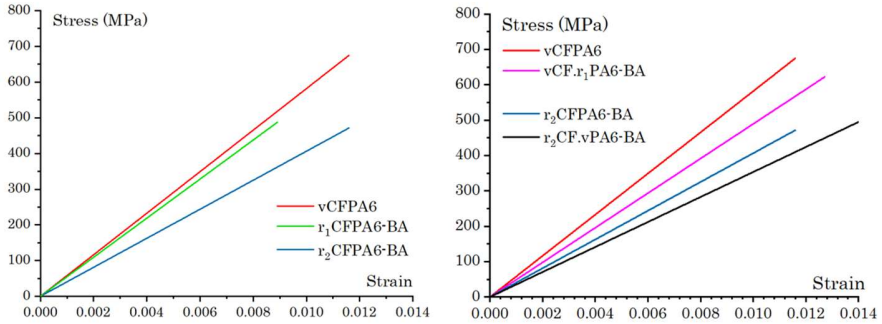

Figure 8. These may not exactly match the tabulated averaged results. The results of the tensile tests are recorded in Table 10, and represented graphically in the Figure 9 bar charts.

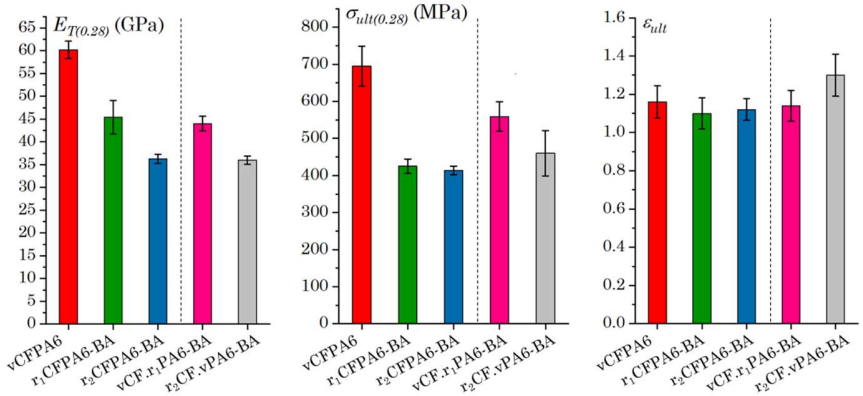

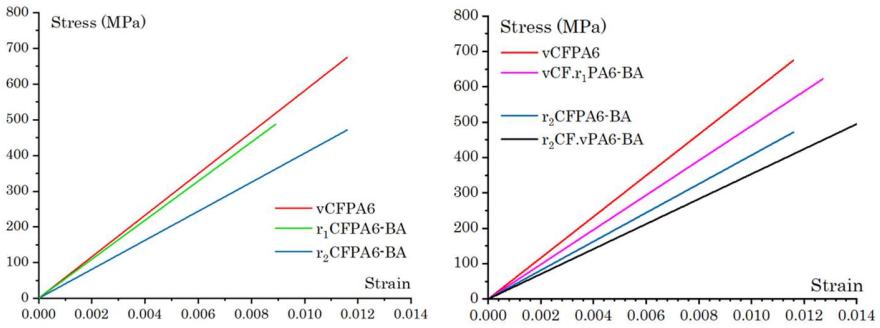

Figure 8. *Left* - Representative stress-strain plots obtained from tensile test of CFPA6-FA as a function of recycling loop. *Right* - Representative stress-strain plots obtained from tensile test of r_2CF.vPA6 and vCF.r_1PA6. Representative plots from vCFPA6 and r_2CFPA6-BA are added for reference.

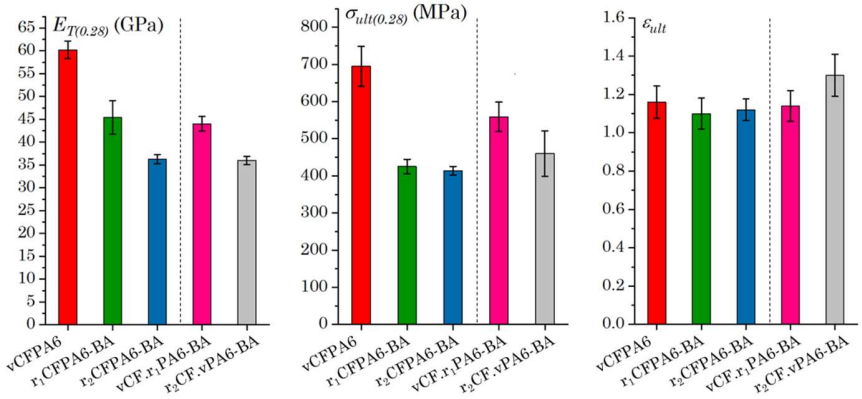

Figure 9. Bar charts showing the normalised tensile stiffness, ultimate tensile strength and ultimate tensile strain of CFPA6-BA as a function of recycling loop, and the constituent exclusion specimens vCF.r_1PA6-BA and r_2CF.vPA6-BA.

Table 10. Average mechanical performance data collected from tensile tests of CFPA6-BA after each recycling loop, and the constituent exclusion specimens vCF.r_1PA6-BA and r_2CF.vPA6-BA. The mechanical performance achieved

	$E_{T(0.28)}$	$\sigma_{ult(0.28)}$	ε_{ult}	ρ	Vf_F
	GPa	MPa		MPa	%
vCFPA6	60.2 (3.18)*	695 (7.75)	1.16 (7.24)	1.09 (8.38)	27.7 (4.61)
r_1CFPA6-BA	45.4 (8.02)	425 (4.67)	1.10 (8.61)	1.13 (6.93)	30.3 (11.1)
r_2CFPA6-BA	36.3 (2.78)	414 (2.66)	1.12 (5.10)	1.16 (2.87)	29.2 (0.91)
vCF.r_1PA6-BA	44.1 (3.67)	559 (7.80)	1.10 (8.61)	1.14 (6.65)	30.1 (1.64)
r_2CF.vPA6	36.0 (10.2)	460 (13.1)	1.30 (10.1)	1.20 (6.9)	29.7 (15.7)

* Coefficient of variance

σ_{ult} was determined as the maximum stress and ε_{ult} refers to the corresponding strain. E_T was determined by taking the gradient of the linear-elastic region section of bounds 0.001 < ε < 0.003. $E_{T(0.28)}$ and $\sigma_{ult(0.28)}$ denote the tensile stiffness and ultimate tensile strength normalised to a 28 % Vf_F, following the rules of mixture.

Tensile specimens exhibited a typical linear-elastic response followed by rapid, brittle failure. Statistical variance between data sets was determined using a Kruskall-Wallis test. To the author's best knowledge, the mechanical performance achieved by vCFPA6 is currently the highest achieved for any aligned, discontinuous carbon fibre thermoplastic composite in the literature. Similarly, to the authors best knowledge, the recycled specimens achieved a higher performance than any recycled discontinuous carbon fibre composite in the literature.

The brittle failure exhibited by all specimens suggested that the IFSS between the CF and PA6 enabled effective load transfer between fibres and matrix resulting in significant fibre fracture. The IFSS between CF and PA6 is typically around 40 – 50 MPa, as reported in the literature [23], this resulted in a critical fibre length of approximately L_c = 0.3 mm. For vCF, this meant that all the fibres were above L_c and could be maximally loaded. Despite this being an approximation, as the exact IFSS of the fibre and matrix used was unknown, the value can be assumed accurate and therefore for vCF all fibres were above the L_c.

vCFPA6-BA has a significantly higher tensile stiffness and ultimate tensile strength than the subsequent specimens. After the first recycling loop the tensile stiffness and ultimate tensile strength decreased by 25 % and 39 %, respectively. After the second recycling loop the ultimate tensile strength and the ultimate tensile strain remained statistically unchanged, however, the tensile stiffness dropped by a further 20 %. Composite stiffness is fibre dominated property, which suggests a successive decrease in fibre alignment as a function of recycling. The second recycling loop did not result in an ultimate tensile strength reduction.

Reduction in composite strength could be a result of either, or a combination of: a) a decrease in intrinsic polymer strength; b) a decrease in fibre-matrix adhesion; c) fibre breakage producing a higher proportion of fibres below the critical fibre length; or d) the presence of defects that act as stress-raisers. There is the potential for a strength reduction from thermal shrinkage, associated with the annealing process, causing residual stresses and microcracks throughout the composite. However, there are no traditional annealing stages present in the remanufacturing process, which is kept consistent throughout each batch, and therefore the only differences in the polymer as a function of recycling that would alter the mechanical properties, related to this, would be variation in crystallinity (ratio of crystal structures) and quantification of this is accounted for with DSC, which shows negligible difference as a function of recycling.

As the polymer characterisation results suggest limited polymer degradation, a decrease in polymer strength can be ruled out as the main contributor. This conclusion is supported by the 40 % decrease in ultimate tensile strength observed in the r_2CF.vPA6-BA specimens, as presented in Figure 8 and Table 10. Despite it containing virgin polymer, the strength reduction is marked; equivalent to decreased observed in the r_2CFPA6-BA specimen. Compared with vCFPA6, vCF.r_1PA6 exhibited a reduction in tensile stiffness and ultimate tensile

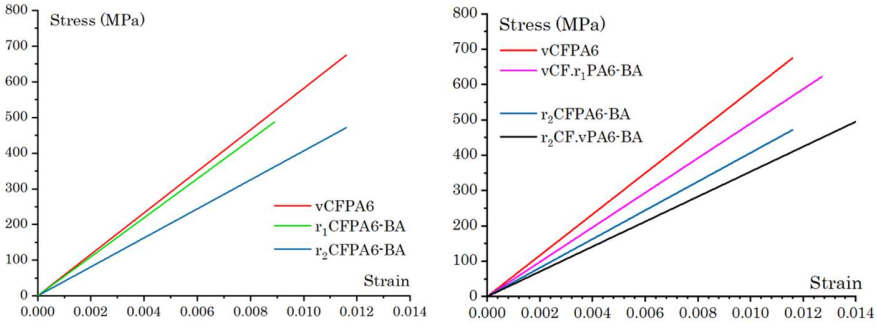

strength of 27 % and 20 % respectively but achieved a similar strain, see

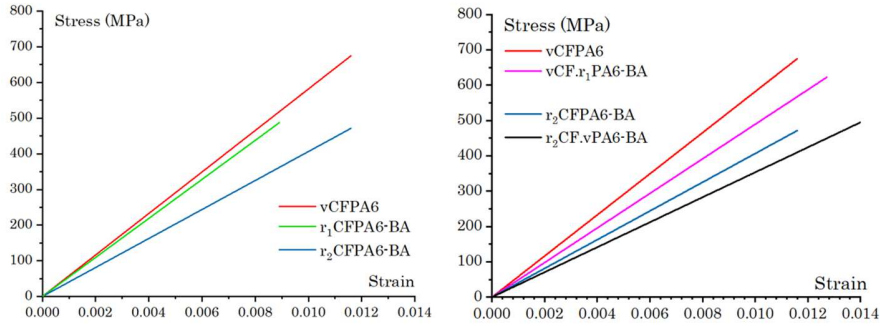

Figure 8 and Table 10. The assumption made was that because both specimens contained vCF preforms, any differences must be caused primarily by the matrix. However, there was a variance in the areal weights produced by the alignment process, preforms in the vCF.r_1PA6 specimens were lower than used in vCFPA6. This meant that the property reduction was because either: a) there is a significant matrix contribution to composite performance, or, b) there is a significant variance in the preform properties produced by the alignment process which causes fluctuations in alignment. The significant drop in properties of the vCF.r_1PA6 specimen, when compared with the vCFPA6 specimen, suggests that variation in fibre deposition and alignment, an aspect of the alignment process itself, is the most likely cause. It is possible that this variation could be exacerbated as a result of recycling, however detailed analysis of the effect of fibre agglomeration/separation on the alignment process would be required to verify this. In any case, this is predominantly a process issue and is separate from any consequences from intrinsic material property degradation which is the focus of this study. The consistency of brittle fracture between recycling loops suggests that fibre-matrix adhesion reduction was not the main contributor either. It is likely that fibre breakage and defects are the cause of the strength reductions, both artefacts of the remanufacturing process.

3.3.3 *Fibre analysis*

The fibre length distribution of preforms made from vCF, and rCF after each recycling loop, are presented in

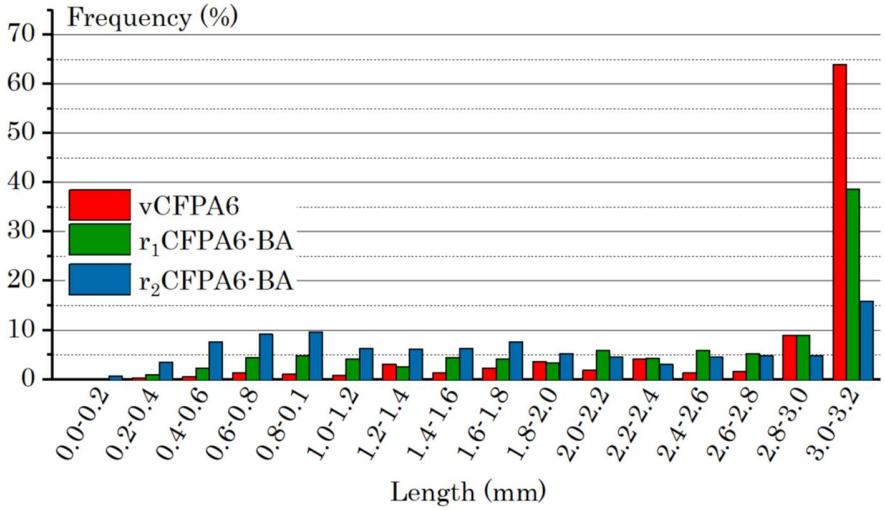

Figure 10. In the vCFPA6 preform sample, 63.9 % of fibres are in the range of 2.8 - 3.2 mm. After the first recycling loop 38.6 % of fibres are in the range 2.8 - 3.2 mm. r_2CFPA6-BA fibre length was more evenly distributed with 0.4 – 0.6 mm, 0.6 - 0.8 mm, and 0.8 – 0.1 mm having 7.5 %, 9.1 % and 9.8 % of the distribution and 3.0 – 3.2 mm representing 15.9 %. The 0.3 mm alignment plate spacing was ≤ 3 % of fibres in each of the recycling iterations, therefore the alignment, and thus the composite stiffness, should not be significantly affected by the evening out of the distribution. This indicates that the decrease in fibre lengths can be ruled out as significant contributors to the reduction in tensile stiffness observed.

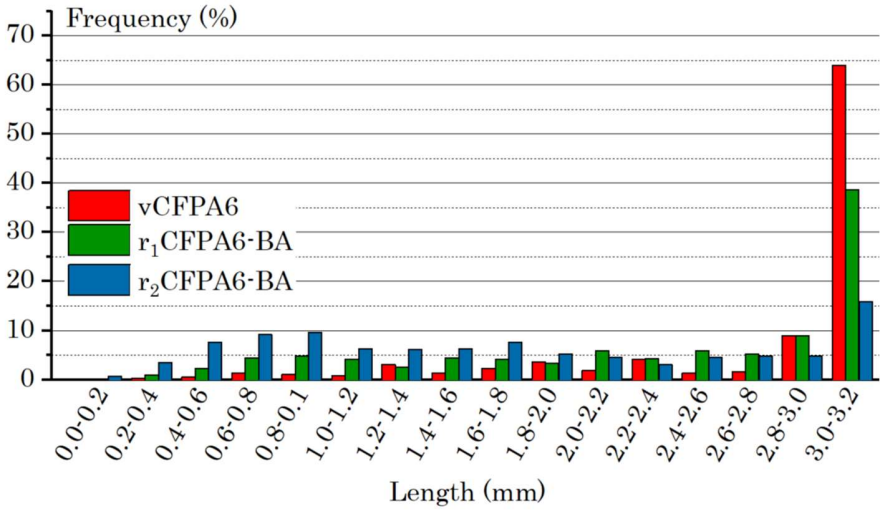

Figure 10. Fibre length distributions of fibre preforms used in vCFPA6, r_1CFPA6-BA and r_2CFPA6-BA.

SEM micrographs were taken of aligned preforms before impregnation of vCFPA6, r_1CFPA6-BA, and r_2CFPA6-BA, see

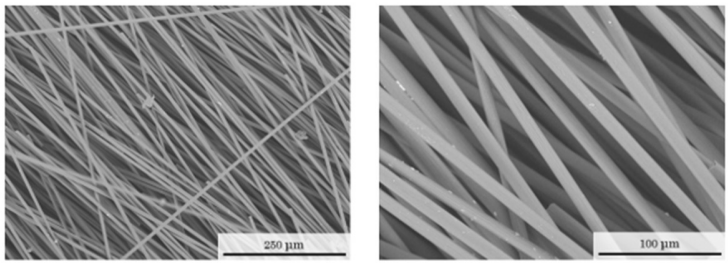

a) SEM micrographs of a preform used in vCFPA6

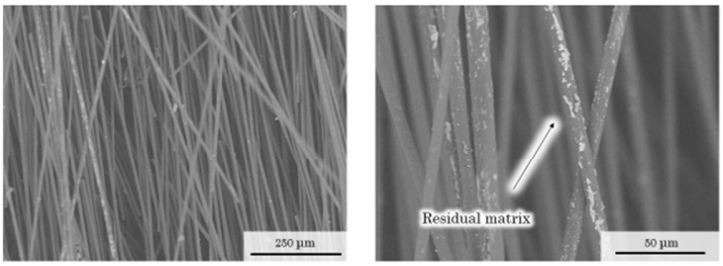

b) SEM micrographs of a preform used in r_1CFPA6-BA

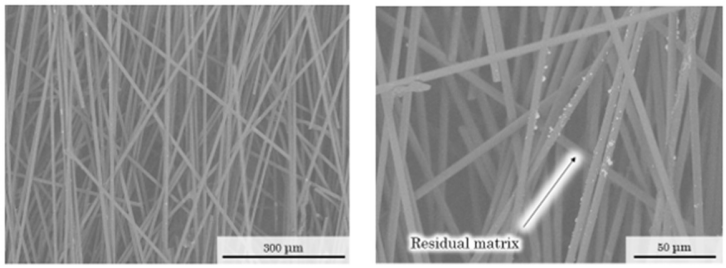

c) SEM micrographs of a preform used in r_2CFPA6-BA

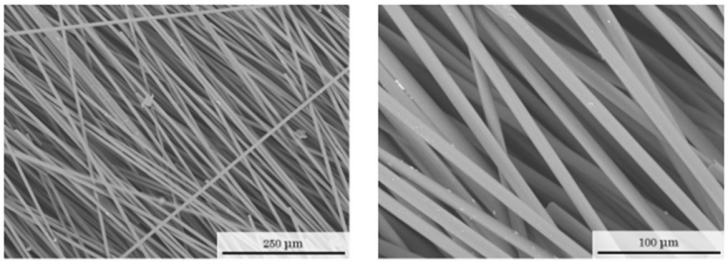

a) SEM micrographs of a preform used in vCFPA6

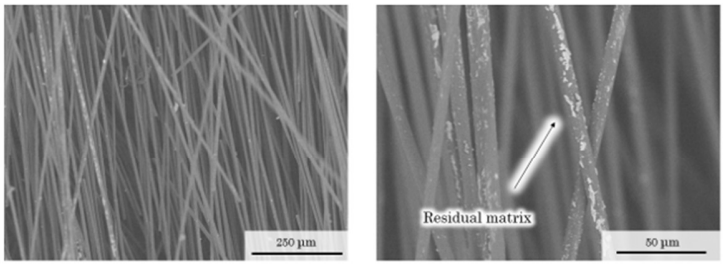

b) SEM micrographs of a preform used in r_1CFPA6-BA

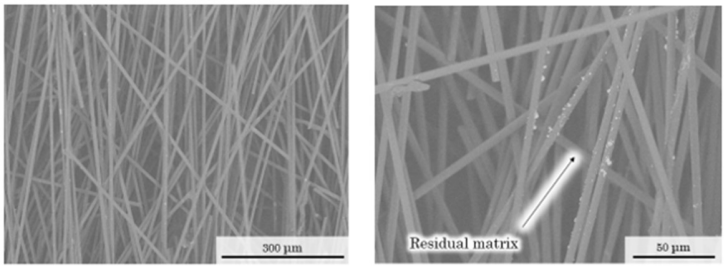

c) SEM micrographs of a preform used in r_2CFPA6-BA

Figure 11a-c.

Figure 11a shows the vCFPA6 preform with clean surfaces in both magnifications.

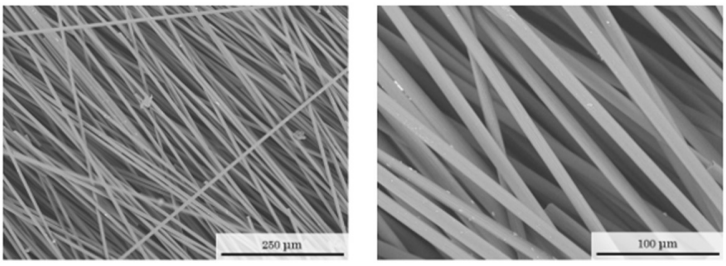

a) SEM micrographs of a preform used in vCFPA6

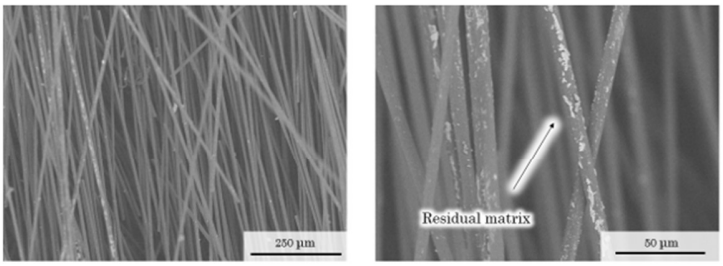

b) SEM micrographs of a preform used in r_1CFPA6-BA

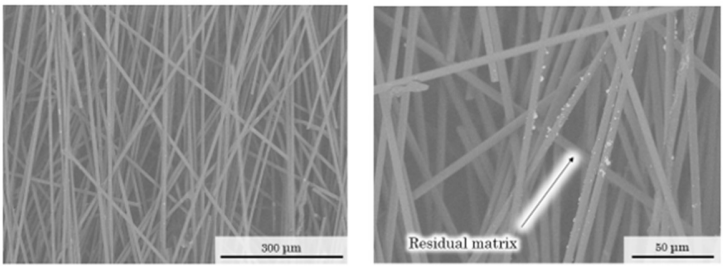

c) SEM micrographs of a preform used in r_2CFPA6-BA

Figure 11b shows the r_1CFPA6-BA preform with a coating in residual matrix adhered to the fibre surface. The micrographs of

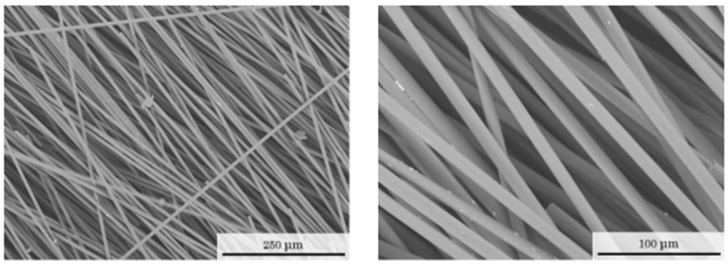

a) SEM micrographs of a preform used in vCFPA6

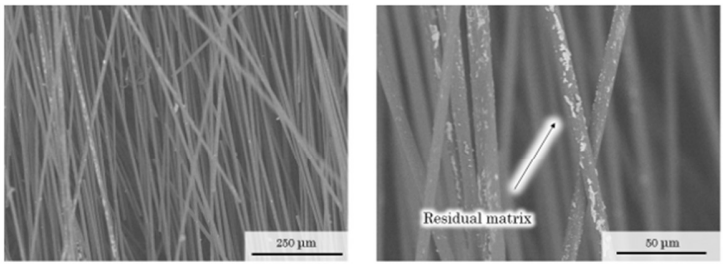

b) SEM micrographs of a preform used in r_1CFPA6-BA

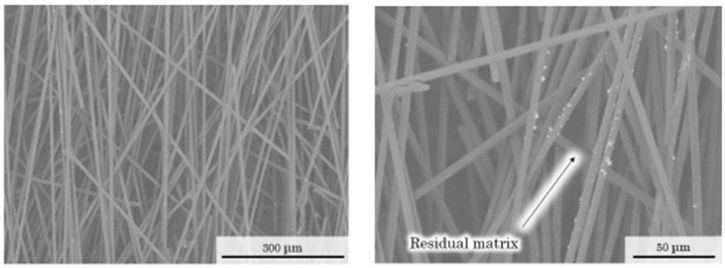

c) SEM micrographs of a preform used in r_2CFPA6-BA

r_2CFPA6-BA,

Figure 11c, show the same residual matrix but in qualitatively unchanged quantities to r_1CFPA6-BA. It is possible that the PA6 residue acted as a form of sizing that increased the IFSS. However, this did not significantly affect the ultimate tensile strength, as observed in previous studies. There is a successive increase of fibre misalignment in the micrographs which reflects the successive decrease in tensile stiffness, however, this may be due to handling of the preform samples during SEM sample preparation.

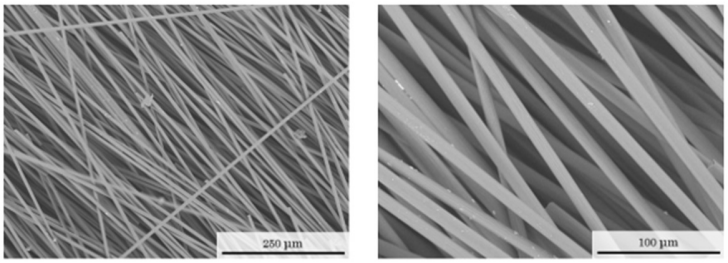

a) SEM micrographs of a preform used in vCFPA6

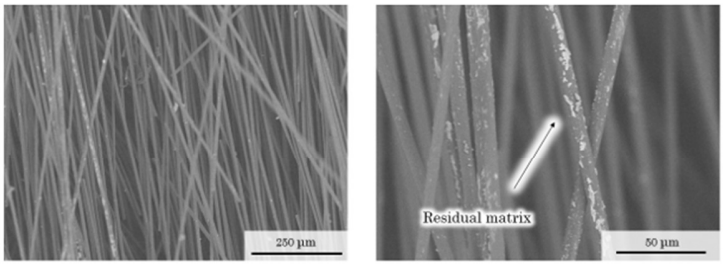

b) SEM micrographs of a preform used in r_1CFPA6-BA

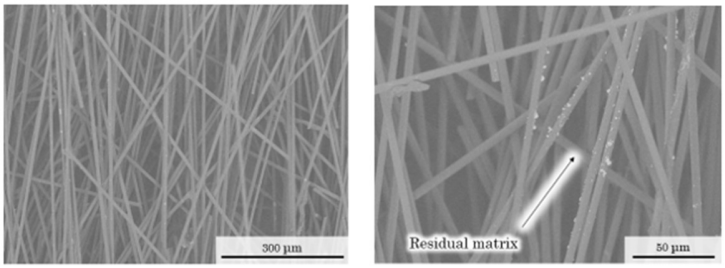

c) SEM micrographs of a preform used in r_2CFPA6-BA

Figure 11. (a-c) Preform cuttings taken from aligned preforms, of each recycling loop, before impregnation. r_1CFPA6-BA and r_2CFPA6 -BA show slight deposition of residue on fibre surface which is deemed to be unwashed matrix.

3.1.2 *Fractography*

SEM micrographs of vCFPA6, r_1CFPA6-BA, and r_2CFPA6-BA fracture surfaces are shown in

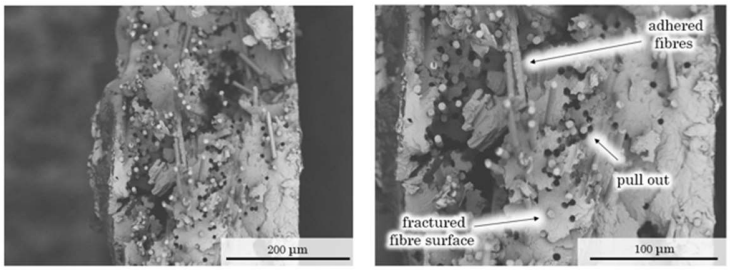

a) SEM micrographs of a vCFPA6 fracture surface

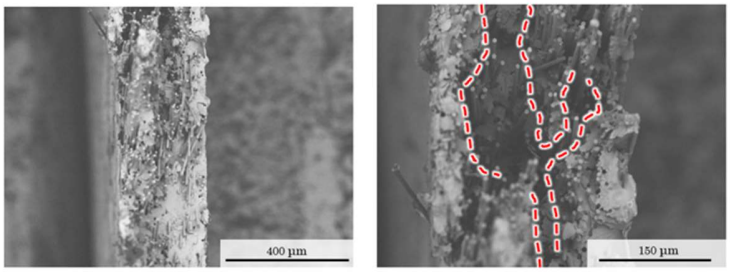

b) SEM micrographs of a r_1CFPA6-BA fracture surface

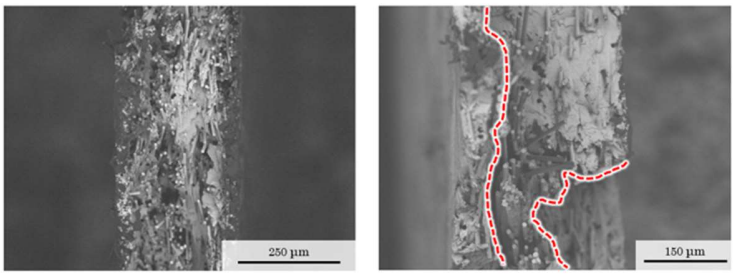

c) SEM micrographs of a r_2CFPA6-BA fracture surface

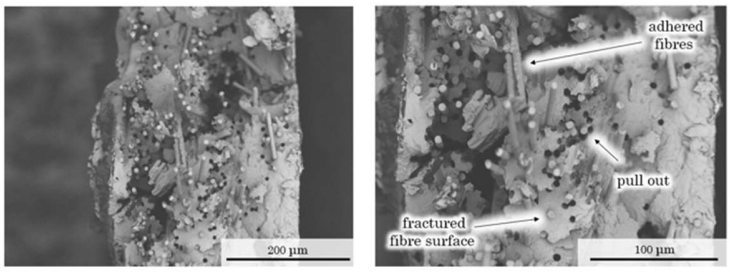

a) SEM micrographs of a vCFPA6 fracture surface

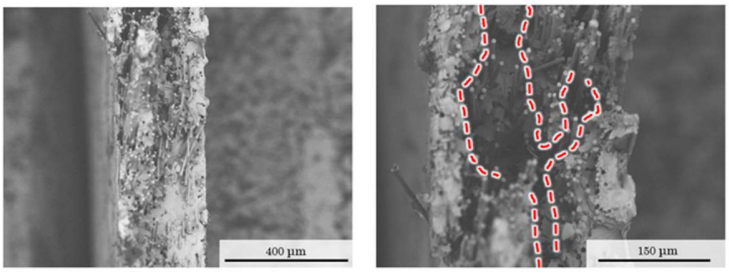

b) SEM micrographs of a r_1CFPA6-BA fracture surface

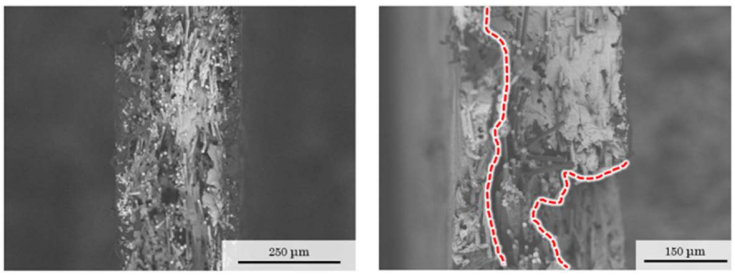

c) SEM micrographs of a r_2CFPA6-BA fracture surface

Figure 12a-b.

Figure 12a shows a typical vCFPA6 fracture surface where some pull-out, fractured fibre ends and well coated fibres are clearly visible. This reflects the linear elastic strain response and brittle failure as the fibres are well adhered to the matrix enabling effective stress transfer.

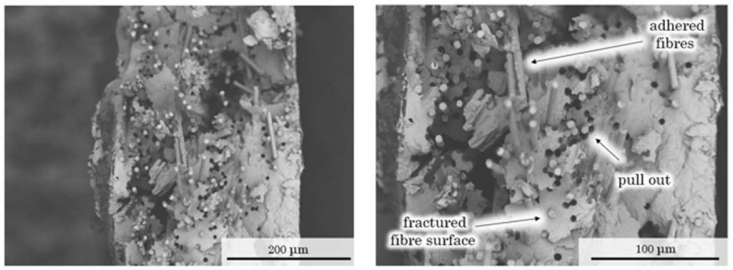

a) SEM micrographs of a vCFPA6 fracture surface

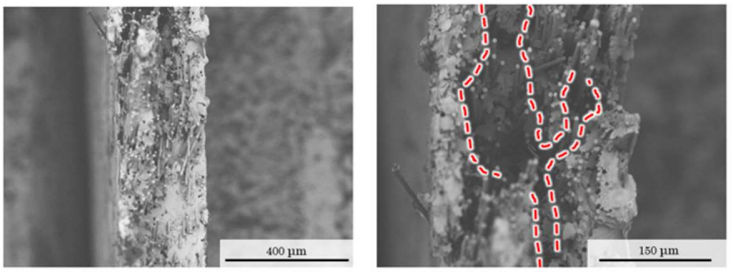

b) SEM micrographs of a r_1CFPA6-BA fracture surface

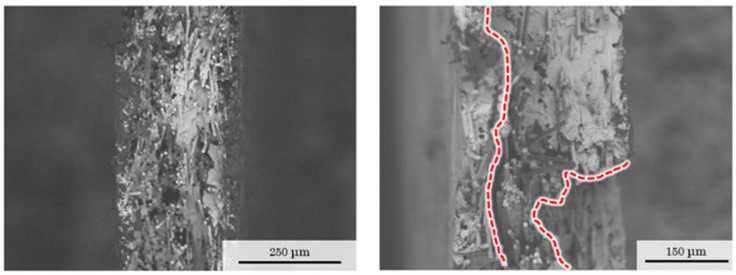

c) SEM micrographs of a r_2CFPA6-BA fracture surface

Figure 12b showed similarly clean matrix crack surfaces however there were large 'valleys; along the cross-section where large sections of composite had cracked off. The large 'valleys' were also visible in the r_2CFP6-BA fracture surface in

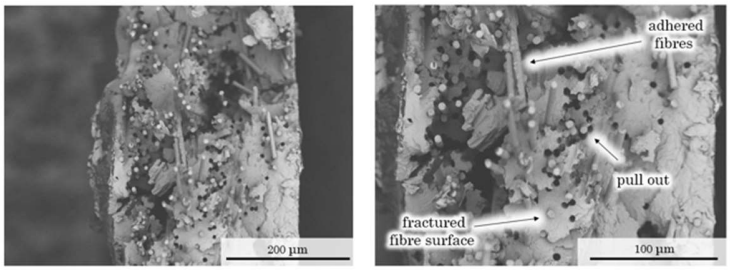

a) SEM micrographs of a vCFPA6 fracture surface

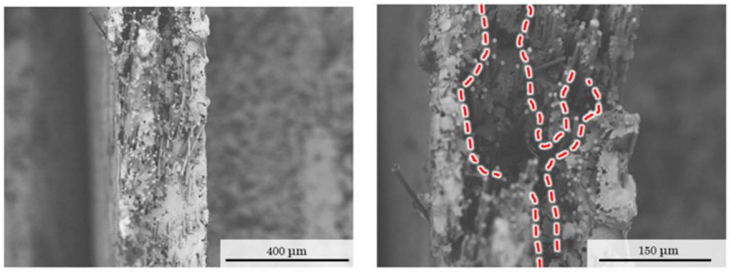

b) SEM micrographs of a r_1CFPA6-BA fracture surface

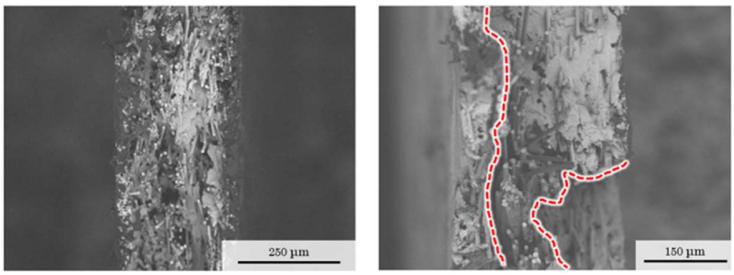

c) SEM micrographs of a r_2CFPA6-BA fracture surface

Figure 12c.

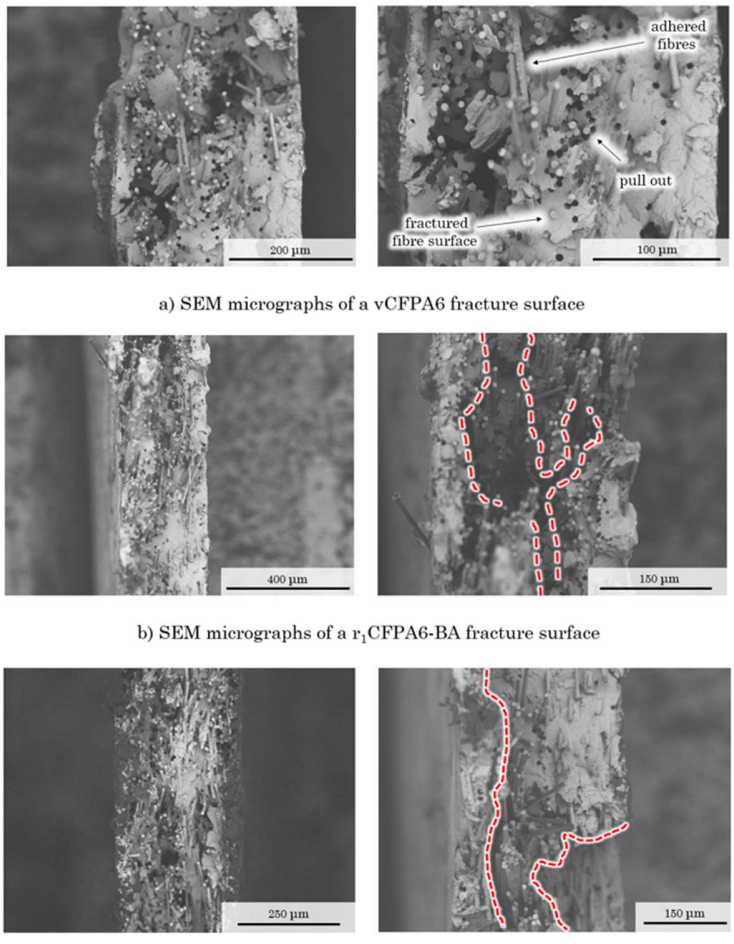

Figure 12. a) A vCFPA6 fracture surface showing pull-out, well coated fibre surfaces and fracture fibre ends. b) A r_1CFPA6-BA fracture surface where large 'valleys' can be seen. c) A r_2CFPA6-BA fracture surface showing more 'valleys'.

The fracture surface 'valleys' suggest that large sections of composite have become detached from the opposite face. This is a consequence of crack propagation past a fibre-dense region, through the matrix-rich regions that typically surround them. The stiffness variation between the two regions initiates and rapidly propagates cracks through the matrix, resulting in reduced tensile strength.

The fibre-dense regions are likely to be caused fibre agglomerations that were not separated by the wet-sonication method. This provides a plausible explanation for the reduction in strength observed in the recycled composite specimens. It also explains the reduction in stiffness as the fibre agglomerations will likely cause misalignment of the surrounding fibres.

3.4 Conclusion

The mechanical performance, polymer properties and fibre properties of virgin and recycled CFPA6 was examined experimentally. The analysis linked macroscopic performance with microscopic fibre surface phenomena, fibre length and polymer behaviour.

DSC analysis indicated that the crystallinity of the polymer was affected by reclamation, however, this was likely due to rapid precipitation on crystal formation and not a consequence of polymer degradation. FTIR spectra also showed no additional peaks or shifts in vibrational frequencies, suggesting unchanged polymer functionalities.

GPC analysis reported successive degradation of the large polymer chains, however, the secondary peak chains were unchanged. HPLC-MS indicated the extraction of small molecules into the supernatant; these masses are substantially less than even small polymer chains. Polymers would have been insoluble in the HLPC carrier solvent and removed before analysis and are therefore not visible in the chromatogram. Small molecules had similar masses to known PA6 additives and their fragment ions.

The CFPA6 specimens showed a total decrease of 39 % (± 3.5) in tensile stiffness and 40.4 % (± 6.1) in tensile strength. The ultimate tensile strain obtained for the CFPA6-BA specimens were statistically invariable as a function of recycling. The ultimate tensile strength reduction, after careful consideration of the potential causes, was most likely due to the presence of fibre agglomerations in the preforms, which formed fibre-dense stress-raisers in the composite, resulting in early failure. Evidence of the fibre agglomerations was observed in the fracture surfaces of the recycled composites. As the composite stiffness is predominantly fibre dependent, it was most likely a result of fibre misalignment caused by the reclamation process.

The fracture surfaces of r_1CFPA6-BA and r_2CFPA6-BA showed relatively deep 'valleys', which suggested that large sections were cleaved during fracture. This indicated the presence of fibre-rich regions surrounded by matrix-dense regions through which cracks easily propagate. Fibre agglomerations were the likely cause of the early failure observed in the recycled specimens. Agglomerations occur during reclamation and are difficult to separate; some are passed through the alignment process without enough prior separation and end up in the preforms. They were not observed in previous studies using an equivalent remanufacturing process, this is likely a consequence of the different separation methods used, suggesting that dry carding is the most effective rCF separation method with regards to minimising agglomerations. The effect of the fibre agglomerations on the mechanical performance indicated that the fibre contribution to composite stiffness and strength was significantly greater than that of the matrix. This makes the issue of reclaimed fibre separation, and pre-treatment prior to remanufacture, of great importance for future investigations and process development.

The mechanical performance achieved by the vCFPA6 specimens was considerable, to the authors knowledge these are the highest mechanical performances achieved by any discontinuous CFPA6 composite in the literature. There was a knockdown in

performance after the first recycling loop, however, the mechanical performance of r_1CFPA6-BA and r_2CFPA6-BA were, to the authors knowledge, the highest observed for any recycled thermoplastic composite, and, for any recycled discontinuous CF composite with either thermosetting or thermoplastic matrices.

4. Acknowledgements

This work was supported by the Engineering and Physical Sciences Research Council through the EPSRC Centre for Doctoral Training at the Advance Composites Centre for Innovation and Science (ACCIS, Grant number EP/L016028/1) and the "High Performance Discontinuous Fibre Composites – a sustainable route to the next generation of composites" project (Grant number EP/P027393/1). All data required for reproducibility are provided within the paper.

5. References

[1] Job S. Composite recycling: Summary of recent research and development 2010.

[2] Composites UK. End-of-Life Solutions for FRP Composites 2015.

[3] Rybicka J, Tiwari A, Leeke GA. Technology readiness level assessment of composites recycling technologies. J Clean Prod 2016;112:1001–12. doi:10.1016/J.JCLEPRO.2015.08.104.

[4] Pickering SJ. Recycling technologies for thermoset composite materials—current status. Compos Part A Appl Sci Manuf 2006;37:1206–15. doi:10.1016/j.compositesa.2005.05.030.

[5] Pimenta S, Pinho ST. Recycling carbon fibre reinforced polymers for structural applications: Technology review and market outlook. Waste Manag 2011;31:378–92. doi:10.1016/j.wasman.2010.09.019.

[6] Oliveux G, Dandy LO, Leeke G a. Current Status of Recycling of Fibre Reinforced Polymers: review of technologies, reuse and resulting properties. Prog Mater Sci 2015;72:61–99. doi:10.1016/j.pmatsci.2015.01.004.

[7] Ellen MacArthur Foundation. The New Plastics Economy: Rethinking the future of plastics. 2016.

[8] Composites Leadership Forum. The 2016 UK Composites Strategy. 2016.

[9] Pillay S, Vaidya UK, Janowski GM. Liquid molding of carbon fabric-reinforced nylon matrix composite laminates. J Thermoplast Compos Mater 2005;18:509–27. doi:10.1177/0892705705054412.

[10] Papaspyrides C, CN K. A Model Study for the Recovery of Polyamides Using the Dissolution/Reprecipitation Technique. Polym Eng Sci 2000;40:979–84.

[11] Gouli S, Poulakis JG, Papaspyrides CD. Solvent recycling of poly(methyl methacrylate) decorative sheets. Adv Polym Technol 1994;13:207–11. doi:10.1002/adv.1994.060130303.

[12] Gutiérrez C, García MT, Gracia I, De Lucas A, Rodríguez JF. The selective dissolution technique as initial step for polystyrene recycling. Waste and Biomass Valorization 2013;4:29–36. doi:10.1007/s12649-012-9131-9.

[13] Hadi J, Najmuldeen F, Ahmed I. Quality restoration of waste polyolefin plastic material through the dissolution-reprecipitation technique. Chem Ind Chem Eng Q 2014;20:163–70. doi:10.2298/CICEQ120526119H.

[14] Achilias DS, Roupakias C, Megalokonomos P, Lappas AA, Antonakou V. Chemical recycling of plastic wastes made from polyethylene (LDPE and HDPE) and polypropylene (PP). J Hazard Mater 2007;149:536–42. doi:10.1016/j.jhazmat.2007.06.076.

[15] Tapper RJ, Longana ML, Yu H, Hamerton I, Potter KD. Development of a closed-loop recycling process for discontinuous carbon fibre polypropylene composites. Compos Part B Eng 2018;146:222–31. doi:10.1016/J.COMPOSITESB.2018.03.048.

[16] Ma Y, Yang Y, Sugahara T, Hamada H. A study on the failure behavior and mechanical properties of unidirectional fiber reinforced thermosetting and thermoplastic composites. Compos Part B Eng 2016;99:162–72. doi:10.1016/j.compositesb.2016.06.005.

[17] Li J, Xia YC. The reinforcement effect of carbon fiber on the friction and wear properties of carbon fiber reinforced PA6 composites. Fibers Polym 2009;10:519–25. doi:10.1007/s12221-009-0519-5.

[18] Pelin CE, Pelin G, Ştefan A, Andronescu E, Dincă I, Ficai A, et al. Mechanical properties of polyamide/carbon-fiber-fabric composites. Mater Tehnol 2016;50:723–8. doi:10.17222/mit.2015.171.

[19] Feng N, Wang X, Wu D. Surface modification of recycled carbon fiber and its reinforcement effect on nylon 6 composites: Mechanical properties, morphology and crystallization behaviors. Curr Appl Phys 2013;13:2038–50. doi:10.1016/j.cap.2013.09.009.

[20] Karsli NG, Aytac A. Tensile and thermomechanical properties of short carbon fiber reinforced polyamide 6 composites. Compos Part B Eng 2013;51:270–5. doi:10.1016/j.compositesb.2013.03.023.

[21] Sang L, Wang C, Wang Y, Wei Z. Thermo-oxidative ageing effect on mechanical properties and morphology of short fibre reinforced polyamide composites-comparison of carbon and glass fibres. RSC Adv 2017;7:43334–44. doi:10.1039/c7ra07884f.

[22] Luo H, Xiong G, Ma C, Li D, Wan Y. Preparation and performance of long carbon fiber reinforced polyamide 6 composites injection-molded from core/shell structured pellets. Mater Des 2014;64:294–300. doi:10.1016/j.matdes.2014.07.054.

[23] Ma Y, Jin S, Zhang S. Plastics, Rubber and Composites Effect of trigger on crashworthiness of unidirectional carbon fibre reinforced polyamide 6 composites Effect of trigger on crashworthiness of unidirectional carbon fibre reinforced polyamide 6 composites. Macromol Eng 2018;8011. doi:10.1080/14658011.2018.1466502.

[24] Do VT, Nguyen-Tran HD, Chun DM. Effect of polypropylene on the mechanical properties and water absorption of carbon-fiber-reinforced-polyamide-6/polypropylene composite. Compos Struct 2015;150:240–5. doi:10.1016/j.compstruct.2016.05.011.

[25] Experimental data on carbon fibre reinforced polyamide-6 composite (CF60/PA-6) under longitudinal and transverse compression loading 2018;1. doi:10.17632/VPR4TFG27J.1.

[26] Ma Y, Jin S, Zhang S. Effect of trigger on crashworthiness of unidirectional carbon fibre reinforced polyamide 6 composites. Plast Rubber Compos 2018;47:208–20. doi:10.1080/14658011.2018.1466502.

[27] Ma Y, Yan C, Xu H, Liu D, Shi P, Zhu Y, et al. Enhanced interfacial properties of carbon fiber reinforced polyamide 6 composites by grafting graphene oxide onto fiber surface. Appl Surf Sci 2018;452:286–98. doi:10.1016/j.apsusc.2018.04.274.

[28] Wu S-H, Wang F-Y, Ma C-CM, Chang W-C, Kuo C-T, Kuan H-C, et al. Mechanical, thermal and morphological properties of glass fiber and carbon fiber reinforced polyamide-6 and polyamide-6 clay nanocomposites. Mater Lett 2001;49:327–33.

[29] Ude AU, Ratnam CT, Azhari CH. The effect of composition of carbon fibre on the mechanical and morhpological properties of carbon fibre reinforced polyamide 6 (PA6/CF) 2007:31–40.

[30] Botelho E., Figiel L, Rezende MC, Lauke B. Mechanical behavior of carbon fiber reinforced polyamide composites.

Compos Sci Technol 2003;63:1843–55. doi:10.1016/S0266-3538(03)00119-2.

[31] Iwamoto R, Murase H. Infrared Spectroscopic Study of the Interactions of Nylon-6 with Water. J Polym Sci Part B Polym Phys 2003;41:1722–9.

[32] TenCate Advanced Composites. TenCate Cetex ® TC910 - Product Data Sheet 2018.

[33] Yu H, Longana ML, Swolfs Y, Wisnom MR, Potter KD. Hybrid effect of carbon/glass composites as a function of the strength distribution of aligned short carbon fibres. 17th Eur Conf Compos Mater 2016:26–30.

[34] Painer D, Lux S, Siebenhofer M. Recovery of Formic Acid and Acetic Acid from Waste Water Using Reactive Distillation. Sep Sci Technol 2015;50:2930–6. doi:10.1080/01496395.2015.1085407.

[35] Höhne GWH, Hemminger WF, Flammersheim H-J. Differential Scanning Calorimetry. Berlin, Heidelberg: Springer Berlin Heidelberg; 2003. doi:10.1007/978-3-662-06710-9.

[36] Solvay L-AF, Lame O, Seguela R, Millot C, Fillot L-A, Lame • Olivier, et al. Assessment of polyamide-6 crystallinity by DSC: Temperature dependence of the melting enthalpy. J Therm Anal Calorim 2015. doi:10.1007/s10973-015-4670-5.

[37] Bergström J, Bergström J. Experimental Characterization Techniques. Mech Solid Polym 2015:19–114. doi:10.1016/B978-0-323-31150-2.00002-9.

[38] Socrates G. Infrared and raman characteristic group frequencies : tables and charts. John Wiley & Sons; 2007.

[39] Klampfl CW. Mass spectrometry as a useful tool for the analysis of stabilizers in polymer materials. TrAC - Trends Anal Chem 2013;50:53–64. doi:10.1016/j.trac.2013.04.012.

[40] Block C, Wynants L, Kelchtermans M, De Boer R, Compernolle F. Identification of polymer additives by liquid chromatography-mass spectrometry. Polym Degrad Stab 2006;91:3163–73. doi:10.1016/j.polymdegradstab.2006.07.015.